NASA TECHNICAL MEMORANDUM

NASA TM X-907

NASA TM X-907

MEASUREMENTS OF THE EFFECTS OF STATIC MAGNETIC FIELDS ON VHF TRANSMISSION IN IONIZED FLOW FIELDS

by F. P. Russo and J. K. Hughes

Langley Research Center
Langley Station, Hampton, Va.

NATIONAL AERONAUTICS AND SPACE ADMINISTRATION • WASHINGTON, D. C. • MARCH 1964

MEASUREMENTS OF THE EFFECTS OF STATIC MAGNETIC FIELDS ON VHF TRANSMISSION IN IONIZED FLOW FIELDS

By F. P. Russo and J. K. Hughes

Langley Research Center
Langley Station, Hampton, Va.

NATIONAL AERONAUTICS AND SPACE ADMINISTRATION

MEASUREMENTS OF THE EFFECTS OF STATIC MAGNETIC FIELDS ON VHF TRANSMISSION IN IONIZED FLOW FIELDS*

By F. P. Russo and J. K. Hughes

SUMMARY

Ground and flight experiments were conducted to determine if the plasma sheath attenuation at VHF telemetry frequencies could be reduced by the use of longitudinal magnetic fields as indicated by theory. The ground tests were made in the 60-foot vacuum sphere at the Langley Research Center facility with solid-propellant rocket exhausts to simulate reentry plasma. A flight experiment (RAM A2) was made from Wallops Island, Virginia, at 7:30 a.m. e.s.t., on February 21, 1962.

The test model for both experiments was a slender probe with a 2-inch-diameter hemispherical nose followed by a 9° half-angle cone joined to a 9-inch-diameter cylindrical afterbody. The magnetic-field coil assembly was mounted behind a broadband slot antenna located on the forward section of the cone and produced a maximum field strength of 750 gauss on the antenna surface.

The reentry plasma simulator caused a 60-decibel signal loss which was reduced to 40 decibels with the application of the magnetic field. Polar plots of signal strength indicate considerable distortion of the E-plane radiation field due to the ionized exhaust.

Signal-strength measurements from the flight test show approximately 5-decibel attenuation from all receiving stations. There appear to be some variations in signal strength due to the magnetic field but fluctuations due to vehicle motion and the low attenuation encountered make it extremely difficult to obtain a conclusive correlation.

The RAM A2 signal losses of 5 decibels were much lower than the 25-decibel loss experienced by RAM A1 but voltage standing-wave ratio (VSWR) and impedance measurements on both flights indicate that detuning the RAM A1 narrowband slot antenna may be responsible for the large difference in measured signal loss.

INTRODUCTION

The ionized flow fields generated by hypersonic-velocity vehicles seriously impede the transmission of frequencies below plasma resonance. Theoretical studies in reference 1 show that the transmission medium can be modified by suitable orientation of static magnetic fields to allow propagation at the lower

*Title, Unclassified.

frequencies. A theoretical analysis for the case of propagation parallel to the static magnetic field is given in the appendix.

The Langley Research Center undertook, as part of Project RAM (Radio Attenuation Measurements), an experimental investigation of the use of magnetic fields to reduce attenuation at VHF telemetry frequencies. Preliminary ground tests made in the 60-foot vacuum sphere at the Langley Research Center used the free-electron concentration present in a solid-propellant rocket exhaust to simulate a reentry plasma. A flight test was made from Wallops Island, Virginia, on February 21, 1962, with a four-stage solid-propellant rocket vehicle designated RAM A2 (the letter refers to vehicle configuration and the numeral to payload experiment). This experiment was conducted on an ascending trajectory reaching a peak velocity of 17,000 fps at an altitude of 158,000 feet. The data period extends from 150,000 to 300,000 feet.

A sharp-nosed body (referred to herein as a slender probe) was used for both ground and flight tests. The slender probe was previously flown on RAM A1 and experienced a 25-decibel signal loss during the so-called VHF blackout region (the RAM A1 flight results are given in ref. 2). Because of the small shock standoff distance and plasma-layer thickness generated by the slender probe, only moderate magnetic fields are theoretically required to modify the transmission medium. Since the RAM A1 results showed a substantial signal loss which could theoretically be alleviated by magnetic fields, the flight experiment described herein was planned after preliminary ground testing.

The purpose of this report is to determine the feasibility of employing magnetic fields at VHF frequencies by assessment of the ground and flight measurements.

SYMBOLS

B	static magnetic field, webers/meter
E	electric-field intensity, volts/meter
e	electronic charge
H	magnetic-field intensity, ampere-turns/meter
$j = \sqrt{-1}$	
K	dielectric constant
k_0	free-space wave number
m	electron mass
N	number of electrons

$n^2(Z)$	square of index of refraction
t	time
u	mean electron velocity
V	defined by equation (4)
W	defined by equation (5)
$\frac{x}{D_n}$	distance from nose to slot antenna
X,Y,Z	Cartesian coordinates
x,y,z	distance along X-, Y-, and Z-axes
α	attenuation constant, nepers/meter
α_Γ	attenuation constant due to reflection
β	phase shift, radians/meter
γ	propagation constant
ϵ_0	permittivity of free space, 8.854×10^{-12}
ϵ_{ij}	elements of effective dielectric tensor
λ	wavelength, meters
μ_0	permeability of free space, 4×10^{-7}
ν	mean collision frequency of electrons with neutral particles, collisions/second
σ	a-c conductivity
ω	transmission frequency, radians/sec
ω_H	electron gyrofrequency, radians/sec
ω_p	electron plasma frequency, radians/second
ϕ,θ,R	spherical coordinates

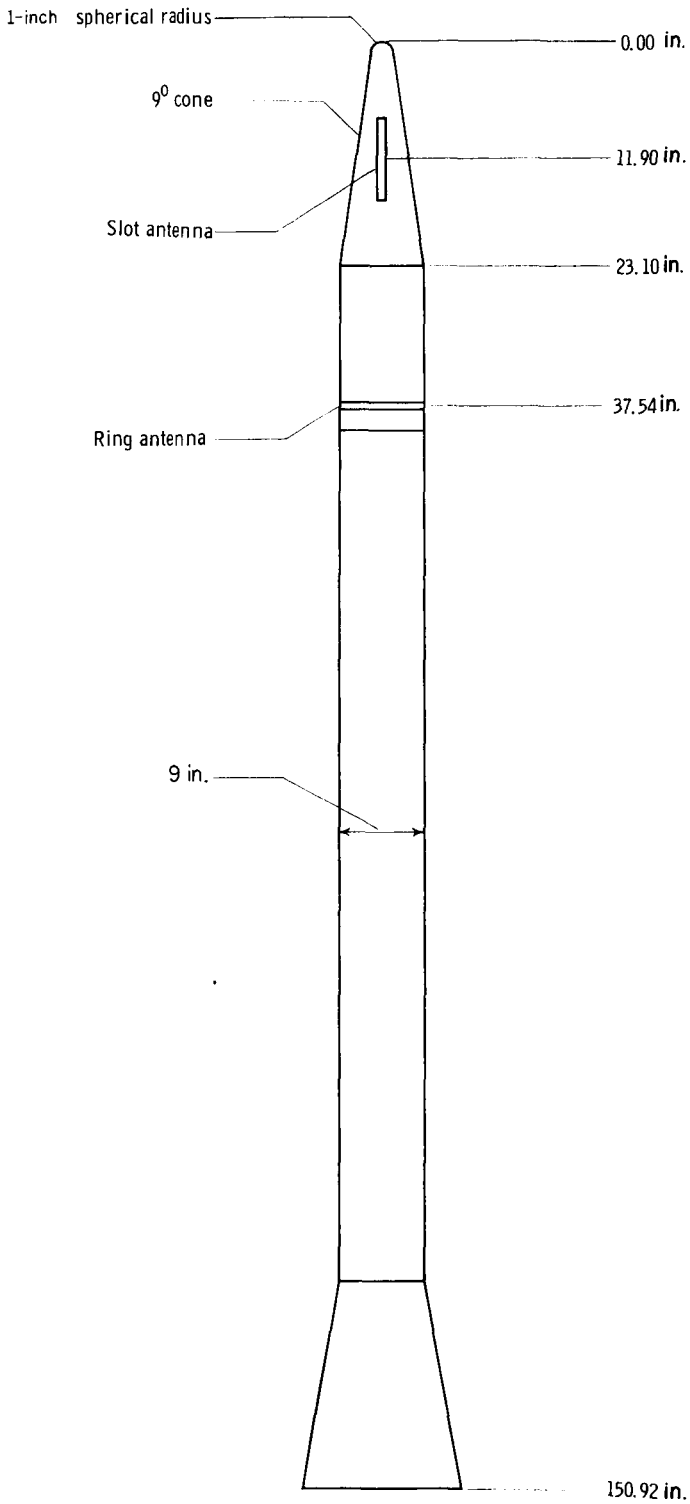

Figure 1.- Sketch of slender probe.

Subscripts:

r	real part of complex number
i	imaginary part of complex number
0	free space

A prime (') denotes differentiation with respect to time.

PROBE DESCRIPTION

The probe shown in figure 1 is a 9° half-angle cone with a 2-inch-diameter nose, a 9-inch-diameter cylindrical midsection, followed by a 10° half-angle flare section at the rear (the ground test model consisted only of the conical nose joined to a 1-foot cylindrical midsection. The flight probe was designed for both static and dynamic stability to insure a low angle of incidence during the data period. Some coning during the high-altitude burning of the fourth stage was anticipated as a result of loss of aerodynamic stability which resulted from the separated flow along the vehicle (ref. 3). A detailed description of the probe is given in reference 4.

MAGNETIC-FIELD COIL ASSEMBLY

Figure 2 shows the conical nose section with the magnetic-field coil assembly located behind a broadband slot antenna.

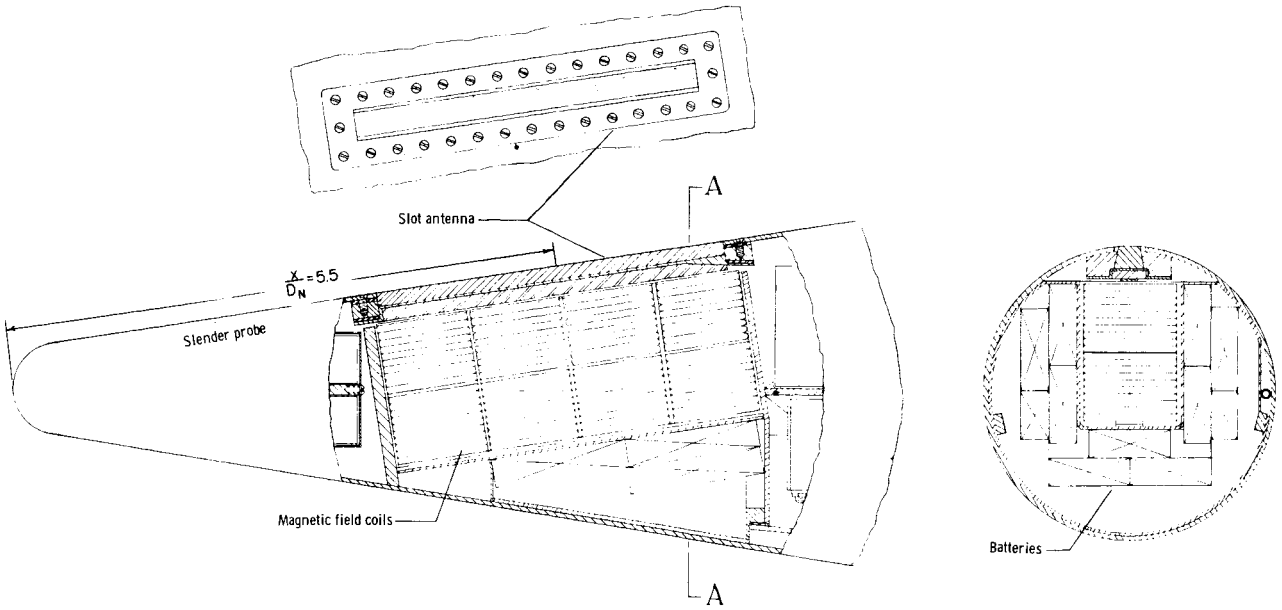

Figure 2.- Slender-probe conical-nose section with magnetic-field assembly behind the forward-slot antenna.

The field was generated by eight 50-turn solenoids which produced a total of 30,000 ampere-turns. Magnetic-field strength and normalized electron gyrofrequency are plotted as a function of distance normal to the slot antenna in figure 3. The flight test was conducted at the two field strengths shown in the figure and is designated as "full" and "half" scale; the sphere tests were conducted at "full" scale only.

SPHERE FACILITY

The 60-foot vacuum sphere facility at the Langley Research Center has as its lower pressure limit 10^{-4} mm Hg. Due to the large volume of the sphere, the gases ejected by the plasma simulators have only a minor effect on the ambient pressure. Propagation measurements made in this facility were conducted in a radio-frequency anechoic chamber (fig. 4) to minimize internal reflections. The absorbing material used provided 28-decibel attenuation at normal incidence for 244.3 mc. Figure 5 shows the probe, rocket motor, and receiving antennas within the anechoic chamber. The probe was electrically isolated from the sphere by use of dielectric support structures and no external connections to the payload were necessary.

SPHERE PAYLOAD INSTRUMENTATION

The self-contained payload consisted of a one-channel NASA FM/AM transistorized telemeter which monitored the current producing the magnetic field. The

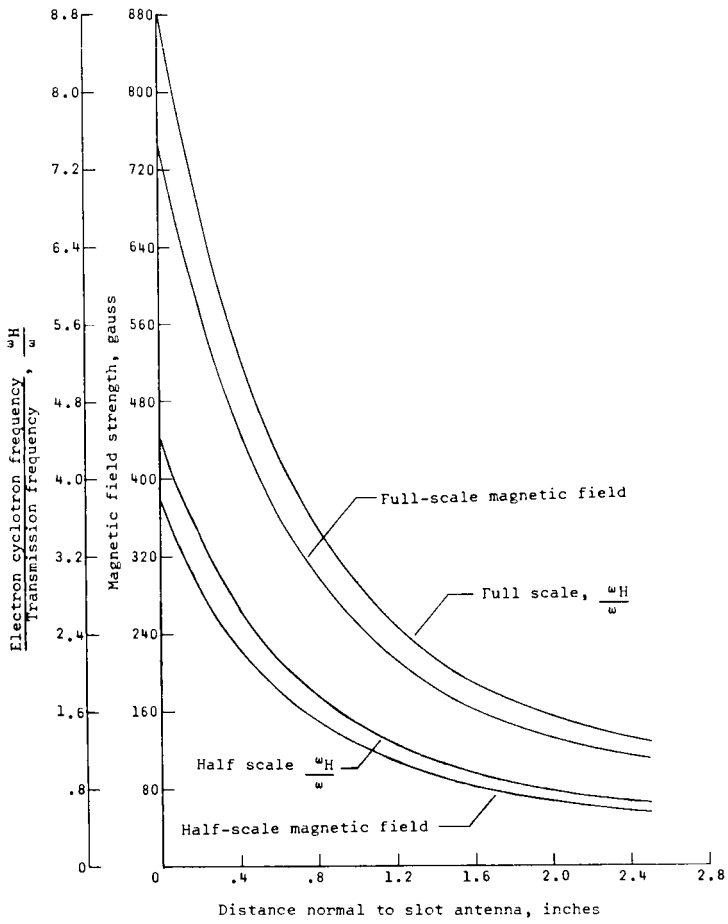

Figure 3.- Variation in magnetic-field strength and electron gyrofrequency normal to the slot antenna.

transmitter operated at 244.3 mc and had a 7-milliwatt nominal-power output into a 50-ohm load. A remote-controlled fiber-optics light pipe was used to switch the telemetry and magnetic field on just prior to rocket-motor ignition. The magnetic field was programed to give an on-off pulse of 1/2-second duration each. Provision to rotate the probe antenna about its longitudinal axis permitted antenna patterns to be taken of the E-plane radiation field. A synchronous marker pulse allowed correlation of the slot-antenna position with respect to receiving antenna B in figure 5. The receiving antennas were coupled coaxially to a receiving station outside the sphere.

Signal strength, sphere pressure, and rocket-motor chamber pressure were recorded for each test. Photographic coverage provided qualitative information on rocket-motor performance, and the chamber pressure, when correlated with attenuation measurements, gave the performance characteristics of individual rocket motors. Signal-strength measurements were recorded as calibrated automatic gain control receiver voltages and put on IRIG subcarrier channels. All data were reduced to digital form and processed by an IBM 7090 electronic data processing system.

PLASMA SIMULATOR

The small rocket motor used a 2-pound charge of highly aluminized solid propellant which generated 100 pounds of thrust for 10 seconds with an exit Mach number of 4 and chamber temperature of 6,200° F. The probe antenna, located 18 inches from the rocket motor (fig. 5) stagnated the central luminous flow of the exhaust which previous microwave measurements had shown to be highly ionized (ref. 5). Because of the high-pressure expansion ratio of the exhaust stream, the flow increased to Mach 10 and enveloped the probe in an ionized sheath characteristic of reentry plasmas.

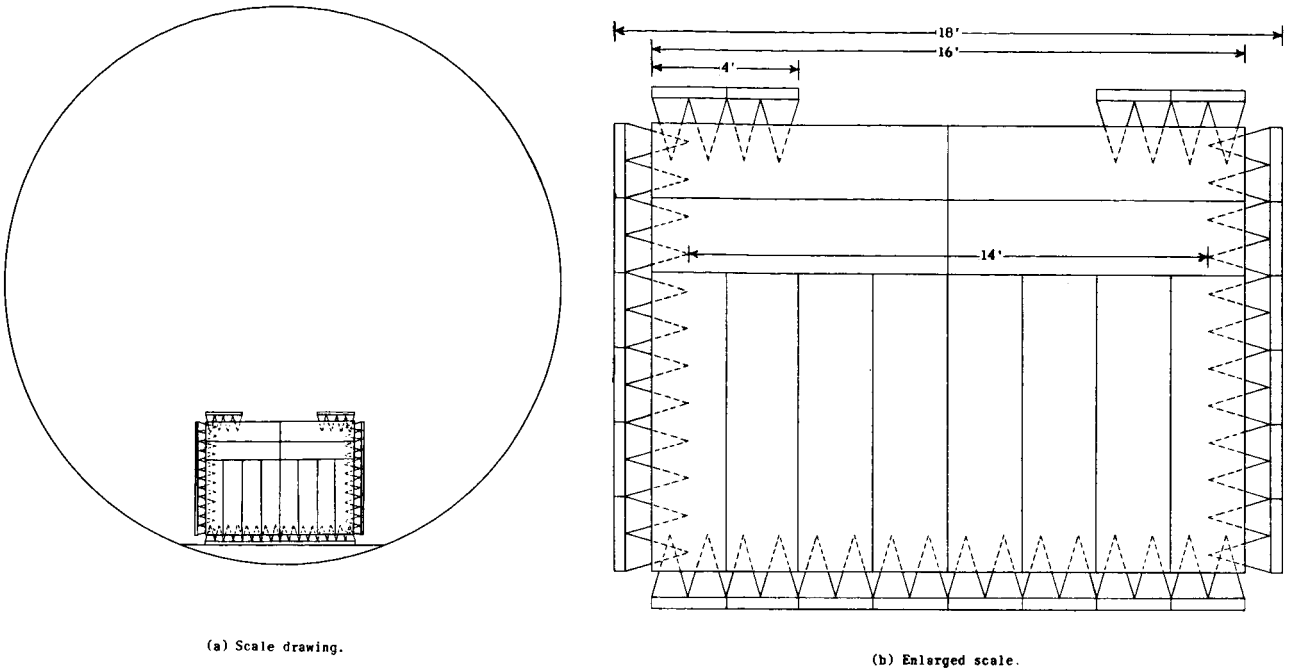

(a) Scale drawing.

(b) Enlarged scale.

Figure 4.- Radio-frequency anechoic chamber within the 60-foot vacuum sphere.

Probe measurements, supplemented by microwave diagnostic surveys, indicated that the plasma simulators produced an average electron density N_e of 3×10^{11} electrons/cm^3 and collision frequency ν of 10^9/sec in the vicinity of the slot antenna; however, because of the variations which exist among individual rocket motors, these values are only representative. It is found that rocket motors which burn beyond the nominal 10 seconds yield a lower degree of ionization. This situation occurred in the second sphere test in which the rocket motor burned for 13 seconds.

Since determination of the actual electron-density gradients normal to the slot antenna did not seem justified at this time, the signal losses in the ionized sheath were computed for a uniform plasma slab 4 centimeters thick (the thickness was determined by the microwave diagnostic surveys discussed in ref. 5). Signal losses computed for the preceding values of N_e and ν by using plane wave theory, showed a total loss of 45 decibels, 14 decibels of which are due to reflection.

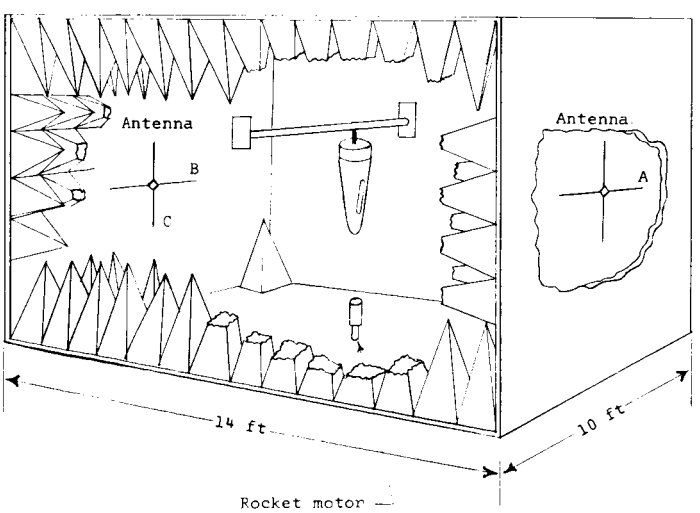

Figure 5.- Probe antenna in the anechoic chamber.

In computing the signal losses for full-scale magnetic field, the electron density and

collision frequency remained constant and the magnetic field was allowed to vary in the direction of propagation. By using the method of reference 6 for computing the losses in the inhomogeneous plasma, the wave equation for normal incidence is written:

$$\frac{d^2\vec{E}}{dz^2} + k_0\left[n^2(Z)\right]\vec{E} = 0 \tag{1}$$

where $n^2(Z)$ = Square of index of refraction. Upon applying the appropriate boundary conditions and separating the resulting equation into its real and imaginary parts, the two following equations result (the $\pm$ sign indicates that the plane wave has been split into two contrarotating circularly polarized waves, designated as the right-hand and left-hand waves):

$$\frac{d^2r}{dz^2} + k_0^2\left(Vr_{\pm} - W_{\pm}s\right) = 0 \tag{2}$$

$$\frac{d^2s}{dz^2} + k_0^2\left(Wr_{\pm} + V_{\pm}s\right) = 0 \tag{3}$$

where r and s are normalized electric-field parameters and

$$V_{\pm} = 1 - \frac{\omega_p^2\left(\omega \mp \omega_H\right)}{\omega\left[\left(\omega \mp \omega_H\right)^2 + \nu^2\right]} \tag{4}$$

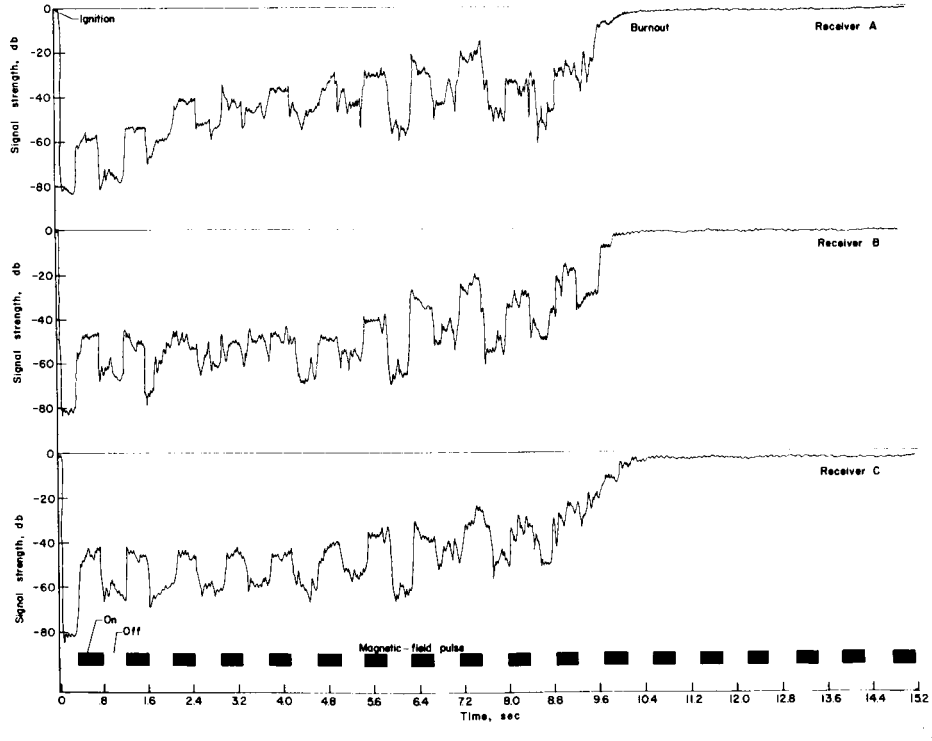

Figure 6.- Ground-test measurements of signal strength with the probe antenna stationary.

$$W_{\pm} = \frac{\omega_p^2}{(\omega \mp \omega_H) + \nu^2} \frac{\nu}{\omega} \qquad (5)$$

The numerical integration was performed on an IBM 7090 electronic data processing system by the Runge-Kutta method (ref. 6). The results obtained indicate that the losses in the ionized sheath are reduced from 45 decibels for no magnetic field to 28 decibels for right-hand circular polarization.

RESULTS AND DISCUSSION

Sphere Tests

The two ground tests were conducted at an ambient sphere pressure of 100 microns prior to rocket-motor ignition. The first test was made with the probe stationary and the slot antenna facing receiver B as in figure 5. Signal-strength measurements for three receiving antennas are shown in figure 6. When the magnetic field was applied, the signal loss was reduced from 60 decibels to 40 decibels, thus showing a 20-decibel enhancement.

During the second test, the probe was rotated at 2 rps. Signal-strength records in figure 7 show essentially the same degree of recovery although the enhancement effects are partially masked by signal fluctuations due to rotation.

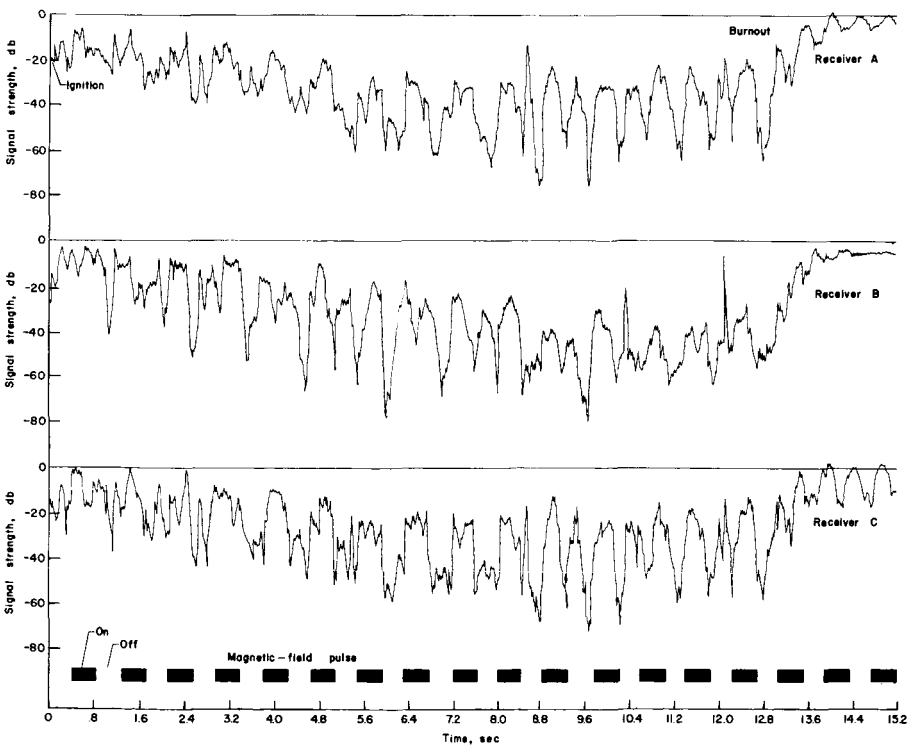

Figure 7.- Ground-test measurements of signal strength with the probe antenna rotated at 2 rps.

Figure 8 shows E-plane radiation patterns plotted from receiver B signal strength in figure 7. The near-circular pattern plotted prior to rocket-motor ignition is

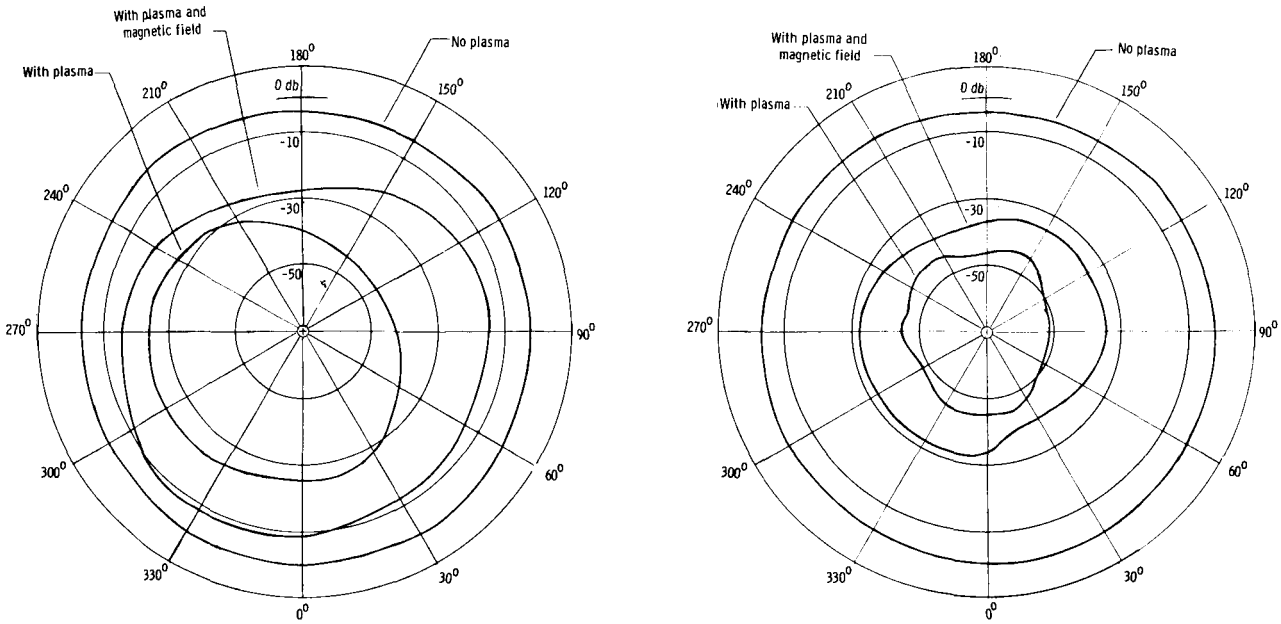

Figure 8.- Ground-test measurements of the E-plane radiation field as a function of the angle ϕ for the case of no plasma, plasma with magnetic field, and plasma without magnetic field.

the free-space reference pattern with antenna position at $\phi = 0^{\circ}$. Under plasma conditions the magnetic field is seen to enhance the entire radiation field although the ionized sheath has markedly altered the radiation characteristics of the antenna.

The preceding results indicate that a substantial improvement in transmission is possible by the application of a longitudinal magnetic field. Experimental results compare favorably with plane wave predictions for the approximate model used although additional losses which may result from antenna detuning and rocket-motor variations were not considered.

Flight Instrumentation

Two broadband UHF antennas were used on the flight payload. The forward-slot antenna radiated a 244.3-mc cw (continuous wave) signal. The ring antenna, located on the cylindrical section, radiated a 240.2-mc telemetry signal. Radiation patterns and bandwidth characteristics for the two antennas are shown in figures 9 to 11. Both transmitters were of similar design with a 2-watt nominal-power output into a 50-ohm load. Telemetry was provided by a nine-channel NASA FM/AM system. Telemetered information included: (1) VSWR and impedance measurements on the forward-slot antenna, (2) magnetic-field coil current, (3) normal

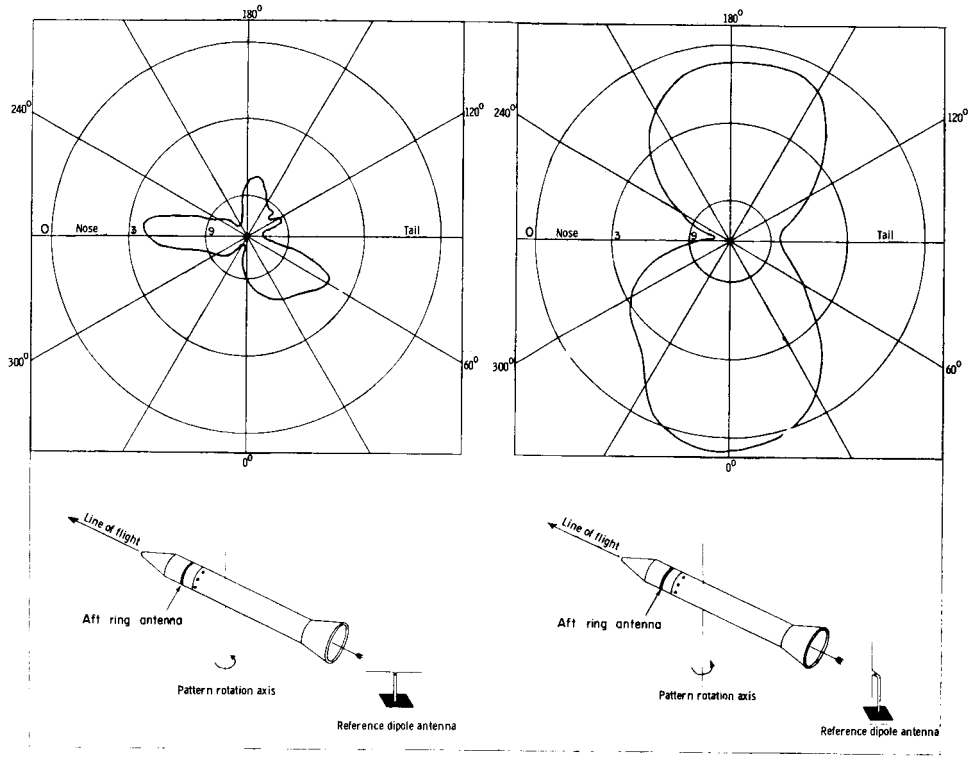

Figure 9.- Aft ring antenna pattern.

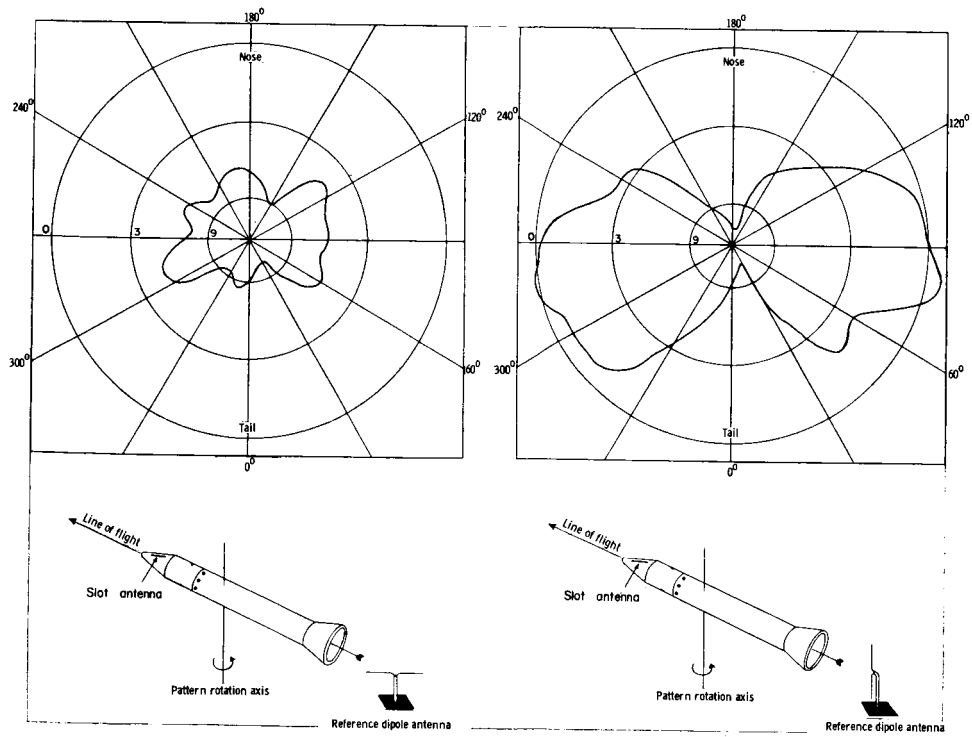

Figure 10.- Forward-slot antenna pattern.

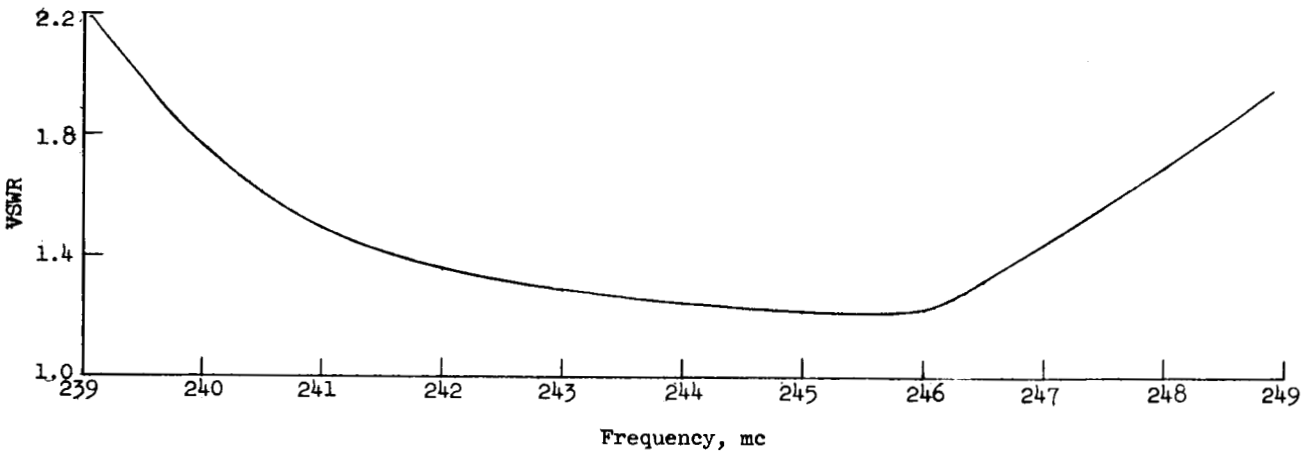

(a) Forward-slot antenna.

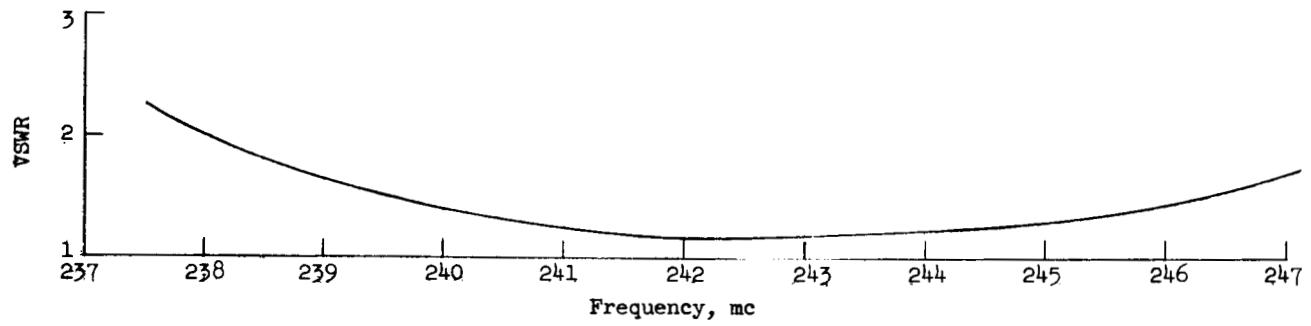

(b) Aft ring antenna.

Figure 11.- Antenna bandwidth characteristics.

and transverse differential nose pressure, (4) normal and longitudinal acceleration, (5) skin temperatures on the nose cone, and (6) sun sensor response. Items 1 and 2 were directly related to the payload experiment while the latter measurements gave information on vehicle performance. The sun sensor, aside from giving roll rate, was used in conjunction with the differential-pressure sensors to determine the slot-antenna orientation with respect to the ground receiving stations.

Figure 12 shows the slant range and look angles from the four receiving stations during the data period. The telemetry information was recorded on magnetic tape only aboard ship and at Wallops Island. Signal strength from both VHF antennas was recorded at all sites. To avoid unwanted signal variation during the data period, no equipment adjustment was allowed after prelaunch calibration. In addition, all receiving stations utilized wide-beam helical antennas which were preset to correspond with the center of the prime data period.

Flight Predictions

Flight-attenuation predictions are made in reference 7 on the basis of nonequilibrium flow effects and computed for a trajectory point of 17,700 fps and 170,000 feet altitude. Figure 13 shows the variations in ω_p, ω_H, and ν from the center of the slot antenna to the shock wave. The curve in figure 14 shows the variation in signal loss along the body based on plane wave theory and includes both finite reaction rates and viscous effects of the boundary layer. In computing the signal losses for an applied magnetic field (see fig. 14), the wave equation was solved by the Runge-Kutta method under conditions of nonuniform plasma and electron gyrofrequencies as shown in figure 13.

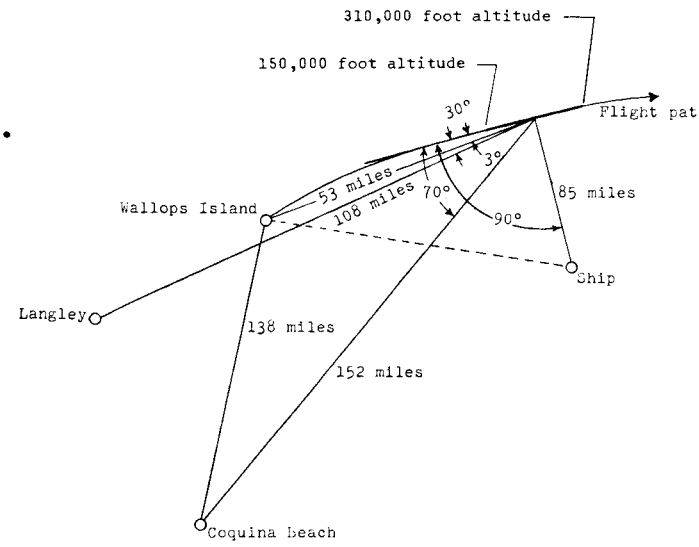

Figure 12.- RAM A2 spatial trajectory during the data period as seen from the ground range.

FLIGHT TESTS

The planned flight trajectory was achieved (see fig. 15) and vehicle performance was normal. Nose-cone temperature did not exceed 750° F and the payload stage angle of incidence varied from 0° to 6° during the prime data period.

Signal-strength measurements from receiving stations at near normal incidence (not shown herein) were similar to the signal-strength record from Langley Research Center (which represents an oblique look angle) shown in figure 16.

Signal loss from each of the two antennas is less than 5 decibels over the entire data period and the forward-slot antenna showed little deviation from its free-space value of 58 / 17° ohms and VSWR of 1.74. Intermittent operation of the magnetic-field switching circuit after fourth-stage ignition was attributed to the high g forces during the 1.5-second thrust period.

Because of the low signal loss, the magnetic field shows only minor signal variations which are partially masked by the fluctuations due to vehicle motion and antenna pattern. The 4-cps variation is the spin rate due to the antisymmetrical antenna pattern. The large spikes occurring between 58 and 60 seconds may be caused by the magnetic field, although their short duration, compared with the total pulse period, is not understood.

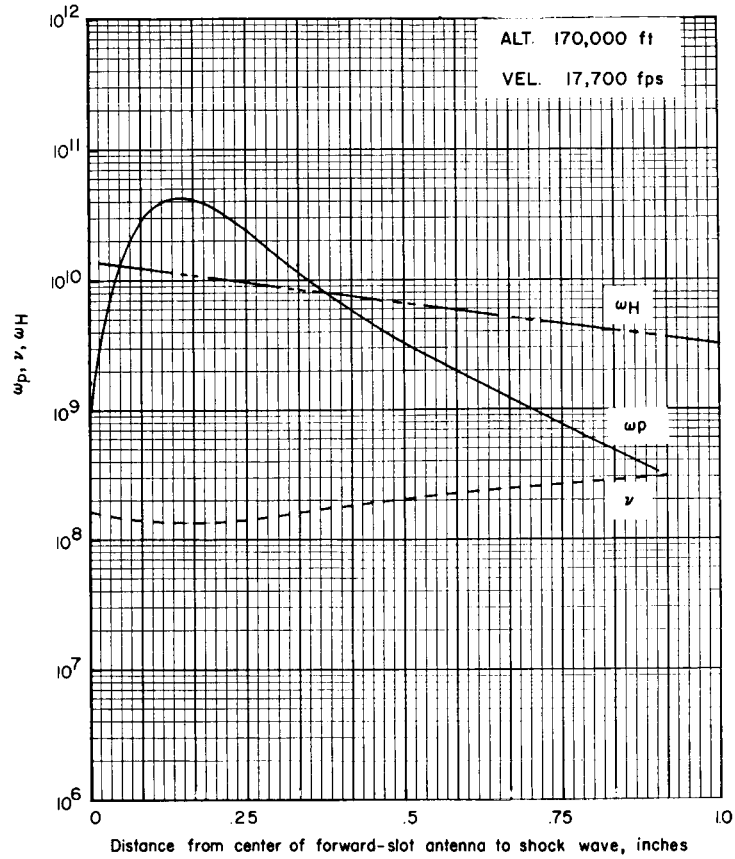

Figure 13.- Theoretical variation in ω_p, ν, and ω_H from the center of the forward-slot antenna to the shock wave.

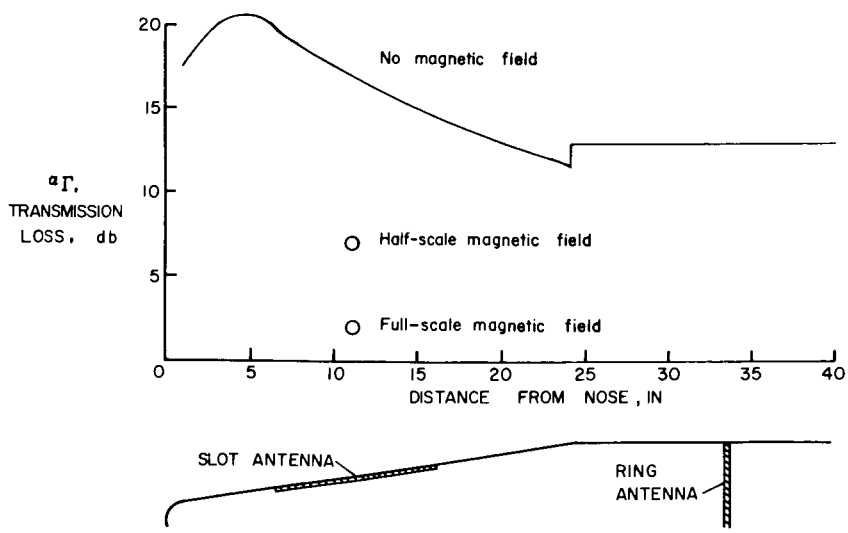

Figure 14.- Theoretical predictions based on plane wave theory for the forward-slot and aft ring antenna.

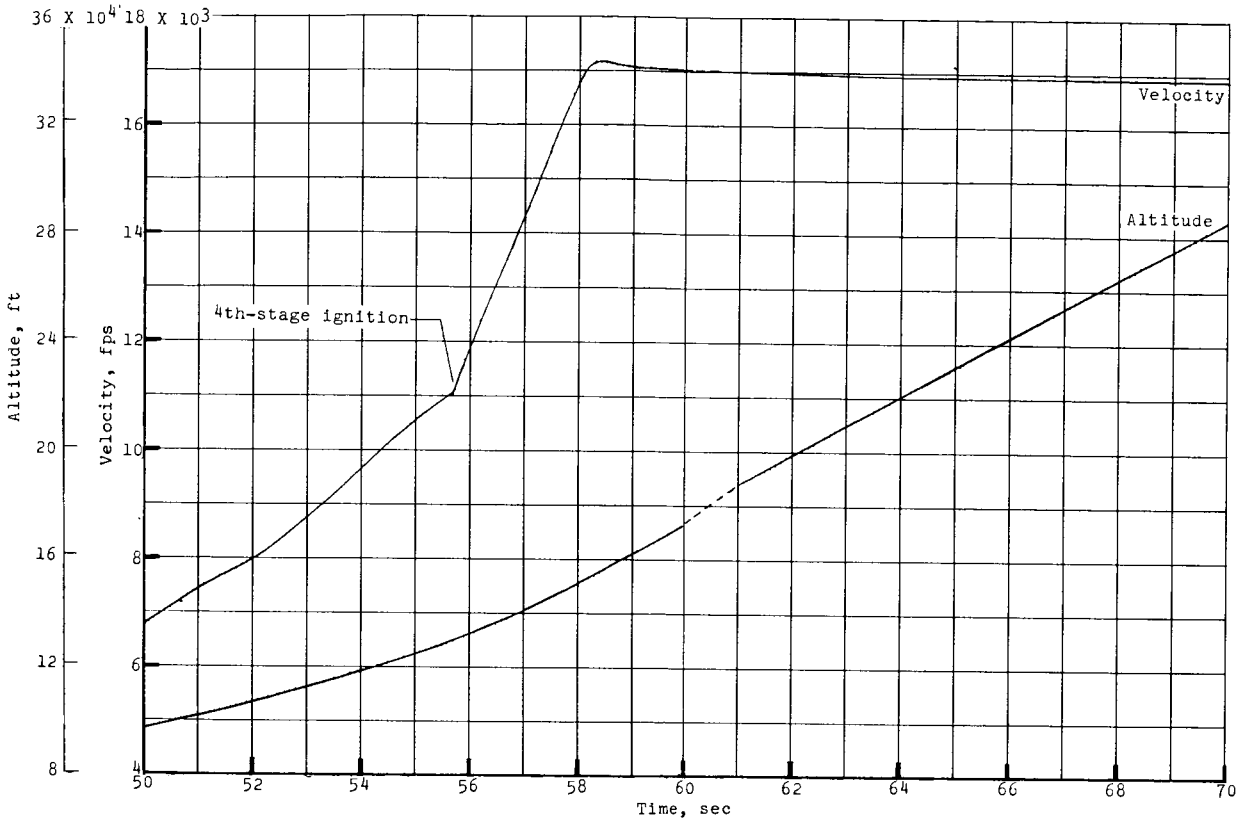

Figure 15.- Time history of velocity and altitude during data period.

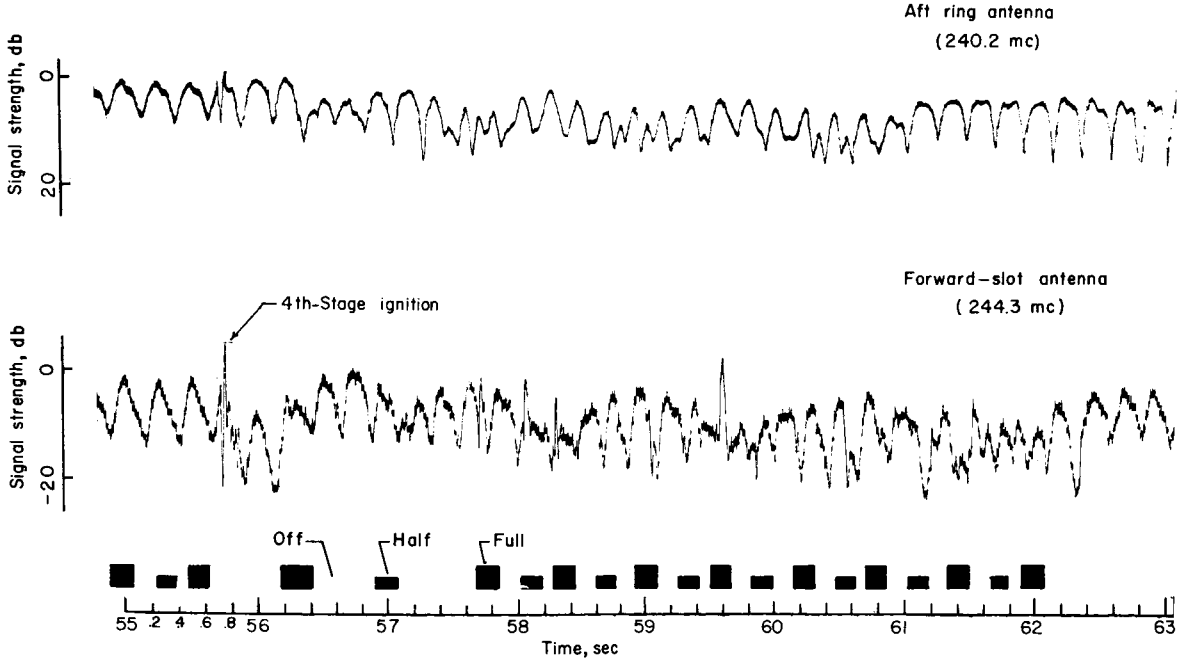

Figure 16.- Signal strength from forward-slot and aft ring antennas received at Langley.

Figure 17 is a comparison of the RAM A1 and RAM A2 flight measurements with two limiting thermodynamic flow models. Both RAM A2 frequencies show attenuations which are between the equilibrium and frozen theoretical plane wave values from reference 8. The greater signal loss for RAM A1 is believed to be due to antenna detuning effects. The RAM A1 slot antenna, as seen in figure 18 is a sharply tuned high Q resonator compared to the RAM A2 slot antenna. During the RAM A1 data period, the VSWR rose to 8 and the slot impedance changed from its free-space value of 50 ohms to 48 /72.8° ohms. This loading of the high Q slot antenna may seriously alter its bandwidth characteristics and radiation efficiency, causing a decrease of radiated power not accountable by VSWR measurements. This was the case for RAM A1 VSWR measurements which indicated a loss of only 4 decibels.

Detuning tests were made with prototype antennas to determine the relative degradation of radiated power. Distilled water and saturated saline solutions were used as the detuning medium. The RAM A1 and RAM A2 slot antennas were each mounted to a self-contained conical nose cone. An outer fiberglass cone, concentric with and spaced 0.25 inch from the probe, contained the solution. A probe covering of thin Mylar prevented direct contact with the solution. Signal

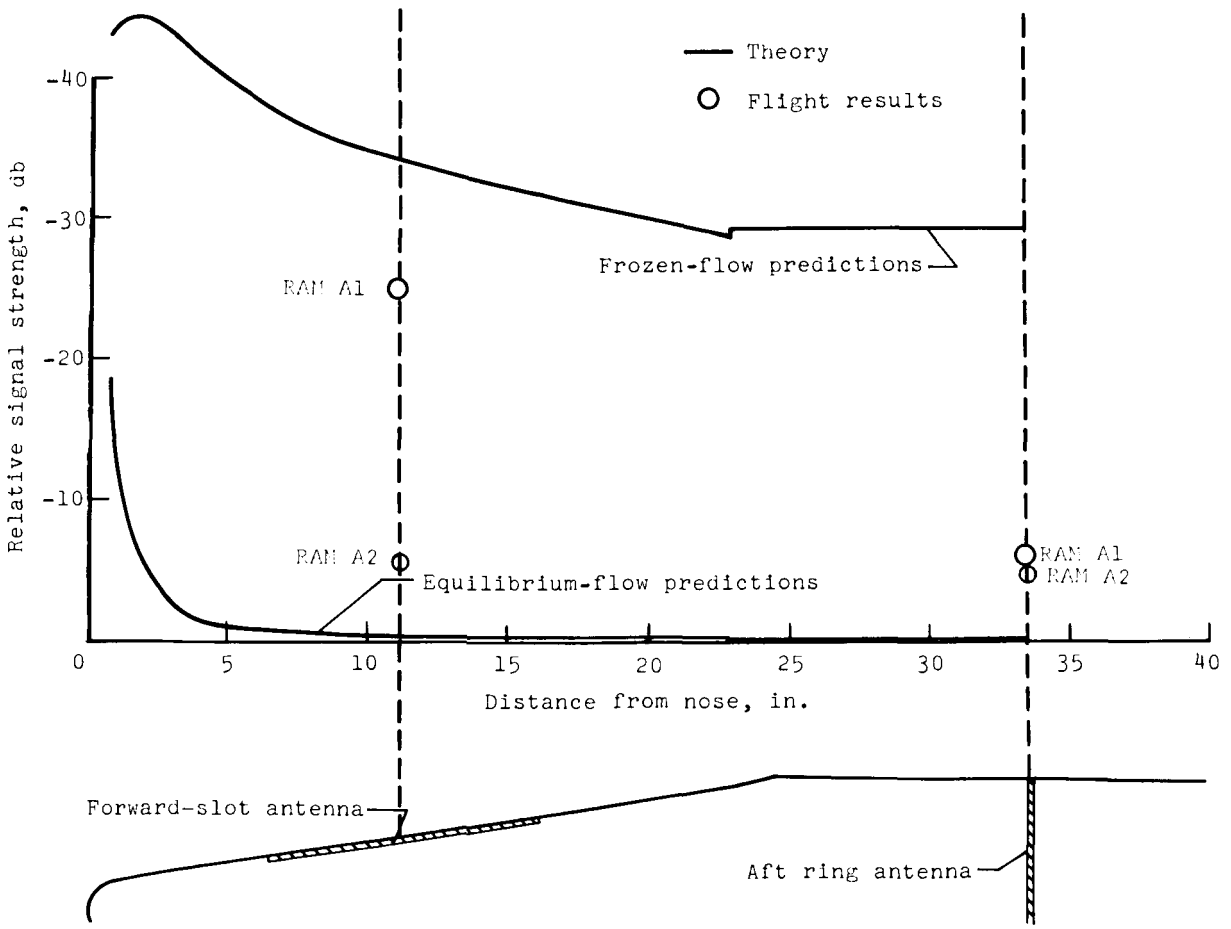

Figure 17.- Comparison of theoretical predictions and flight results at the trajectory point of 158,000 ft and 17,700 fps.

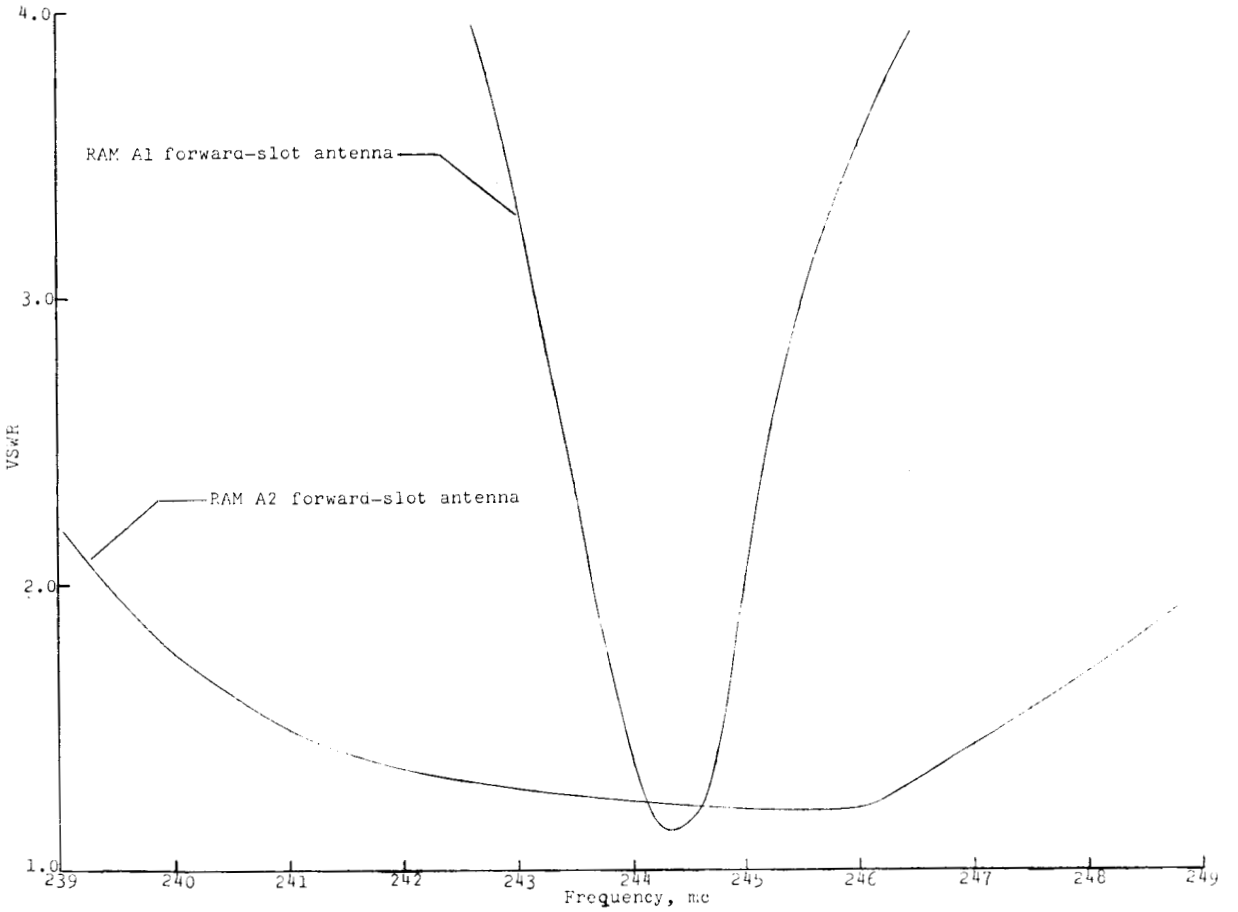

Figure 18.- Comparison of antenna bandwidth characteristics.

strength, VSWR, and impedance measurements were made with 1-watt input power to each antenna. Signal-strength measurements were referred to the free-space signal level of each antenna. This reference level was arbitrarily chosen as 0 decibel. The results of these tests, which are listed in the following table, indicate that the narrowband RAM A1 antenna suffered a 12-decibel greater signal loss than RAM A2 in the same medium.

TABLE I.- VSWR, IMPEDANCE, AND SIGNAL-STRENGTH MEASUREMENTS FOR THE SLENDER-PROBE ANTENNA DETUNING TESTS

	VSWR	Impedance, $Z \angle \phi$	Received signal strength, db
Free space	RAM A1 - 1.45	$60.5 \angle 7.1^\circ$	0
	RAM A2 - 1.2	$44.8 \angle 6.4^\circ$	0
Distilled water	RAM A1 - 19	$37.16 \angle 84.6^\circ$	-24
	RAM A2 - 6.5	$57.7 \angle 72.3^\circ$	-13
Saturated saline solution	RAM A1 - 15	$33.86 \angle 81.0^\circ$	-39
	RAM A2 - 5.5	$54.3 \angle 69.8^\circ$	-27

CONCLUDING REMARKS

VHF transmission characteristics in magnetoionic plasmas were investigated in ground and flight tests.

Attenuation measurements in the ground plasma simulator showed a 20-decibel signal enhancement for a magnetic field of 750 gauss over the antenna surface, and thus indicate the feasibility of the magnetic-field technique. Polar plots of signal strength indicated the magnetic field produced an omnidirectional enhancement in the E-plane radiation field although the ionized sheath markedly altered the radiation characteristics.

The 5-decibel signal loss encountered by RAM A2 was between the theoretical values based on equilibrium and frozen flow predictions for a velocity of 17,700 fps and altitude of 158,000 feet. The forward-slot-antenna impedance showed little change from its free-space value of 58 $\angle 17^{\circ}$ ohms and voltage standing-wave ratio of 1.74. The magnetic field caused only minor signal variations and these were partially masked by fluctuations due to vehicle motion and an asymmetrical antenna pattern. Voltage standing-wave ratio and impedance measurements for RAM A1 indicate that detuning of the narrowband slot antenna may be responsible for the large difference in signal loss between the two flights.

Langley Research Center,
National Aeronautics and Space Administration,
Langley Station, Hampton, Va., October 28, 1963.

APPENDIX

THEORETICAL EFFECTS OF MAGNETOIONIC PLASMAS

The anisotropic behavior of magnetoactive plasmas gives rise to permittivity and conductivity coefficients which are complex tensor quantities. In the case of propagation parallel to the static magnetic field (fig. 19), the familiar Faraday rotation of linearly polarized wave occurs. A window is created below the electron gyrofrequency enabling right-hand circular (RHC) polarized waves to propagate with low attenuation (ref. 1).

The equation of motion for plasma electrons in crossed electric fields E and magnetic fields B is written:

$$\frac{d\vec{u}}{dt} + \nu\vec{u} = \frac{e}{m}\left(\vec{E} + \vec{u} \times \vec{B}\right) \qquad (A1)$$

where $\vec{u}$ is the mean electron velocity, ν is the mean collision frequency of electrons with neutral particles, and e and m are the electronic charge and mass, respectively. The effective dielectric tensor K for the anisotropic medium is given by

$$K = K_r - jK_i \begin{vmatrix} \epsilon_{11} & j\epsilon_{12} & 0 \\ -j\epsilon_{12} & \epsilon_{11} & 0 \\ 0 & 0 & \epsilon_{33} \end{vmatrix} \qquad (A2)$$

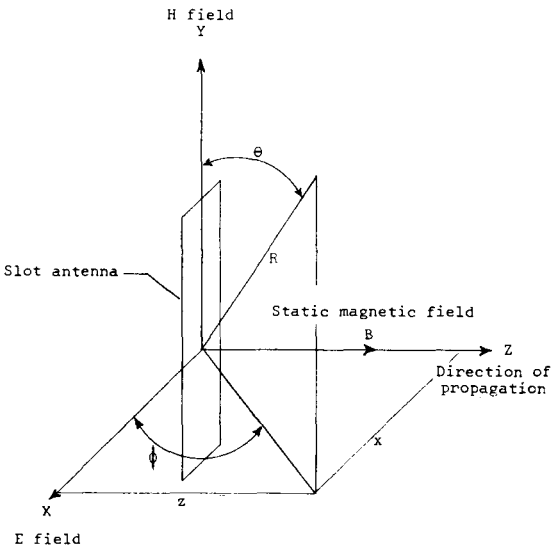

Figure 19.- Magnetic-field orientation with respect to the slotted-antenna coordinate system.

where ϵ_{ij} represents the elements of the dielectric tensor (see ref. 8). Expressing Maxwell's equations in terms of the plasma parameters:

$$\left.\begin{aligned} \nabla \times \vec{E} &= -\mu_0 \frac{\partial \vec{H}}{\partial t} & \nabla \times \vec{H} &= \epsilon\frac{\partial \vec{E}}{\partial t} + \sigma\vec{E} \\ \nabla \cdot \vec{E} &= 0 & \nabla \cdot \vec{H} &= 0 \end{aligned}\right\} \qquad (A3)$$

gives the wave equations for the anisotropic medium:

$$\nabla^2\vec{E} + k_0 K\vec{E} = 0 \qquad (A4)$$

$$\Delta\vec{H} + k_0 K\vec{H} = 0 \qquad (A5)$$

where $k_0 = 2\pi/\lambda$ is the free-space wave number. For plane wave propagation along the Z-axis, equations (4) and (5) have solutions of the form:

$$\vec{E} = \vec{E}_0 e^{j(\omega t - \gamma z)}$$

$$\vec{H} = \vec{H}_0 e^{j(\omega t - \gamma z)} \tag{A6}$$

where the propagation constant

$$\gamma = jk_0 K^{1/2} = \alpha + j\beta \tag{A7}$$

gives the attenuation α and phase constant β of the anisotropic plasma.

For the magnetic field oriented along the direction of propagation, the dielectric tensor K in equation (2) reduces to:

$$K = \epsilon_{11} \pm \epsilon_{12} = 1 - \frac{\omega_p^2}{\omega\left[\left(\omega \mp \omega_H\right) - j\nu\right]} \tag{A8}$$

where the $\pm$ sign indicates that the plane wave has been split into two contra-rotating circularly polarized waves, designated as the right-hand and left-hand waves, respectively. Solving equation (A7) for α and β gives

$$\alpha_\pm = \frac{k_0}{\sqrt{2}}\left(-K_{r\pm} + \sqrt{K_{r\pm}^2 + K_{i\pm}^2}\right)^{1/2} \text{ nepers meter} \tag{A9}$$

$$\beta_\pm = \frac{k_0}{\sqrt{2}}\left(K_{r\pm} + \sqrt{K_{r\pm}^2 + K_{i\pm}^2}\right)^{1/2} \text{ radians meter} \tag{A10}$$

where

$$K_{r\pm} = 1 - \frac{\omega_p^2(\omega \mp \omega_H)}{\omega\left[(\omega \mp \omega_H)^2 + \nu^2\right]}$$

$$K_{i\pm} = \frac{\omega_p^2}{\left[(\omega \mp \omega_H)^2 + \nu^2\right]}\frac{\nu}{\omega}$$

Figure 20 shows the attenuation constant for the RHC polarization as a function of collision frequency for $\omega_H = 0$ and $\omega_H = 8.8 \times 10^9$. The strong

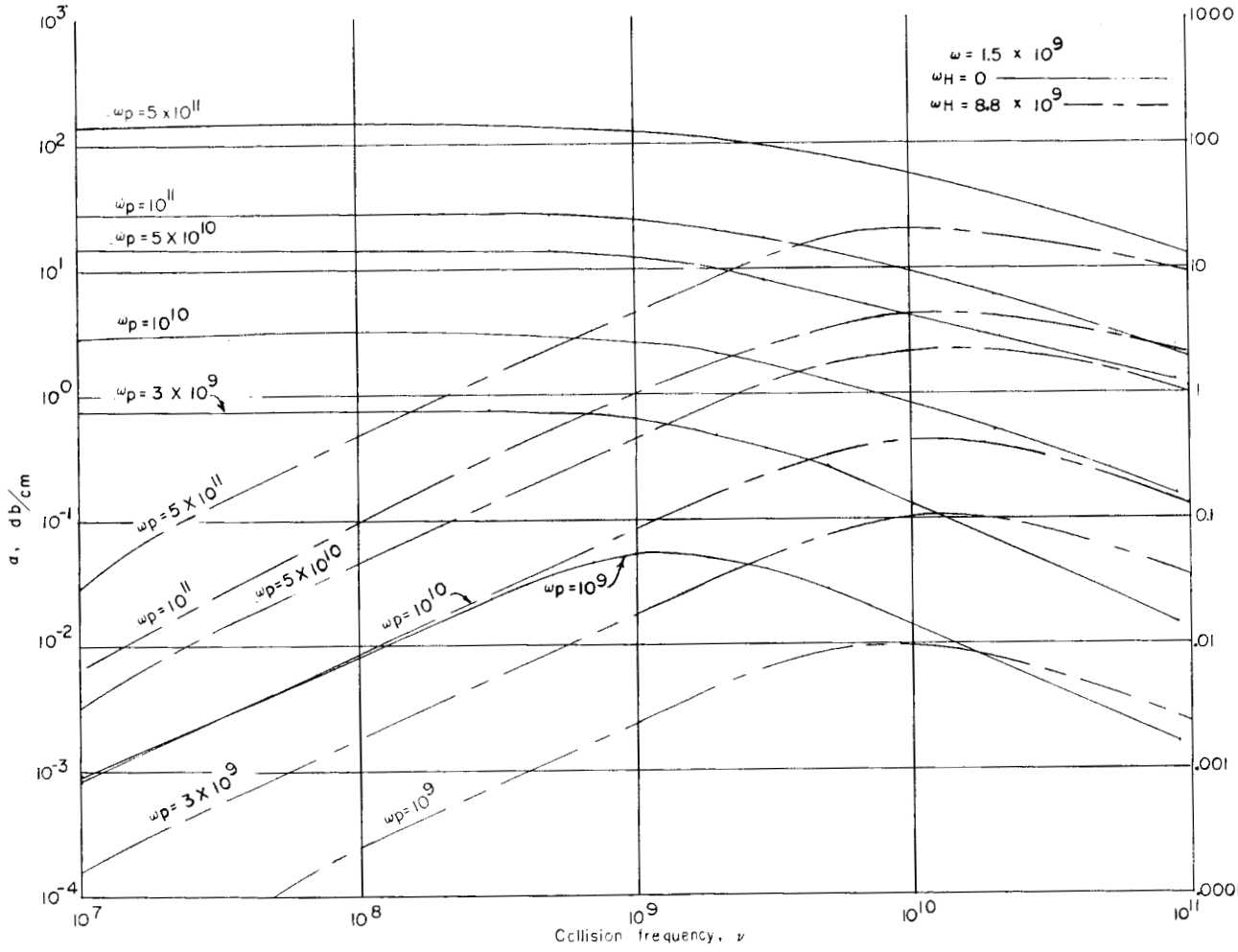

Figure 20.- Attenuation constant for RHC polarized waves as a function of collision frequency.

dependence upon collision frequency indicates a substantial improvement in transmission is realized only when $\omega_H > \nu$. For typical reentry conditions where $\omega_p > \nu > \omega$, the magnetic field must be such that $(\omega - \omega_H)^2 \gg \nu^2$. The altitude dependence exhibited by this technique necessitates the use of stronger fields at the lower altitudes for continuous transmission. The transmission losses given in figure 21 show that, for low values of ν, the losses with applied magnetic field are independent of collision frequency. When $\nu > \omega_H$, the losses approach those for the no-magnetic-field case.

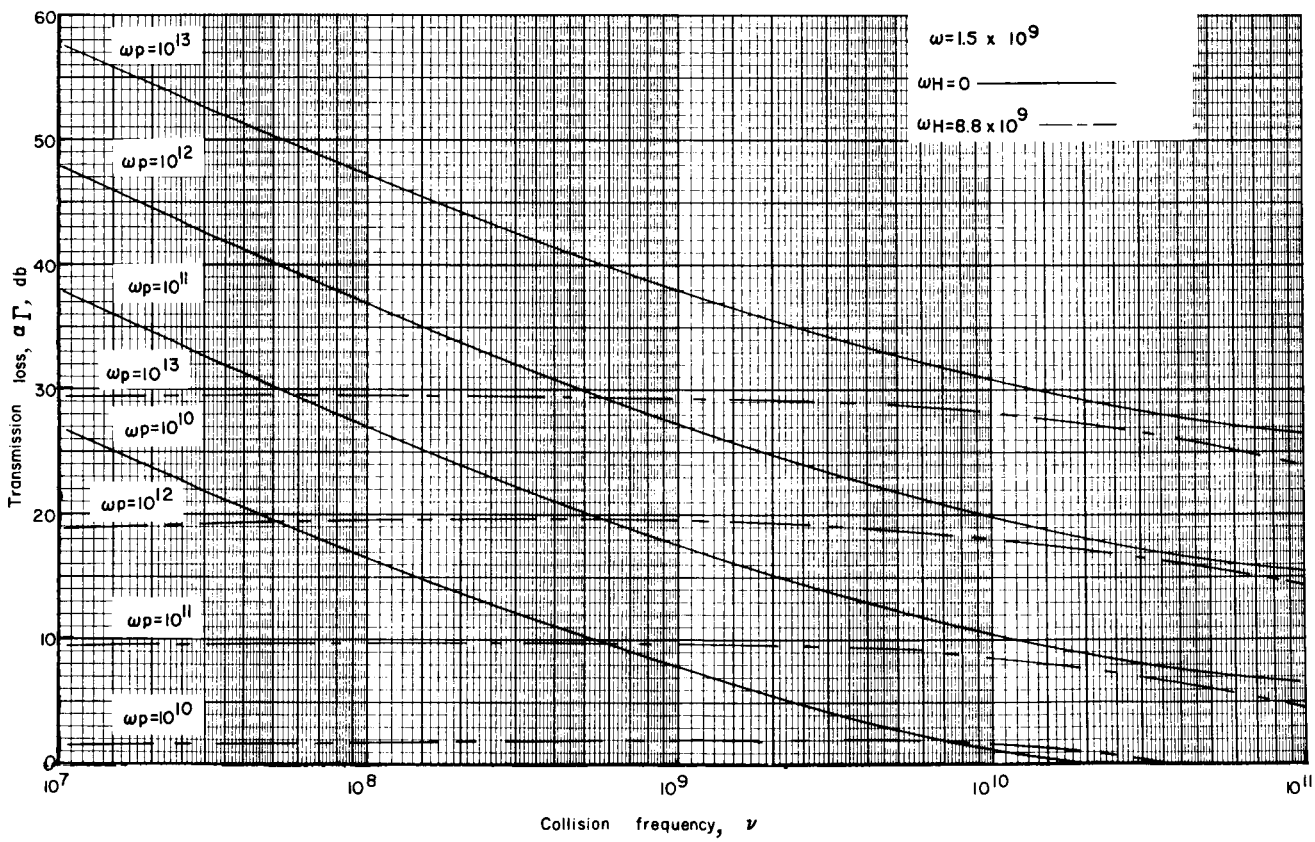

Figure 21.- Transmission loss for RHC polarized waves as a function of collision frequency.

REFERENCES

1. Hodara, H.: The Use of Magnetic Fields in the Elimination of the Re-Entry Radio Blackout. Proc. IRE, vol. 49, no. 12, Dec. 1961, pp. 1825-1830.

2. Sims, Theo E., and Jones, Robert F.: Flight Measurements of VHF Signal Attenuation and Antenna Impedance for the RAM A1 Slender Probe at Velocities Up to 17,800 Feet Per Second. NASA TM X-760, 1963.

3. Falanga, Ralph A., Hinson, William F., and Crawford, Davis H.: Exploratory Tests of the Effects of Jet Plumes on the Flow Over Cone-Cylinder-Flare Bodies. NASA TN D-1000, 1962.

4. Levine, Jack: Performance and Some Design Aspects of the Four-Stage Solid-Propellant Rocket Vehicle Used in the RAM A1 Flight Test. NASA TN D-1611, 1963.

5. McIver, Duncan E., Jr.: 18. Radio-Frequency Signal Attenuation by Plasmas of Rocket Exhaust Gases. A Compilation of Recent Research Related to the Apollo Mission. NASA TM X-890, 1963, pp. 135-144.

6. Swift, Calvin T., and Evans, John S.: Generalized Treatment of Plane Electromagnetic Waves Passing Through an Isotropic Inhomogeneous Plasma Slab at Arbitrary Angles of Incidence. NASA TR R-172, 1963.

7. Huber, Paul W., and Evans, John S.: Theoretical Shock-Layer Plasma Flow Properties for the Slender Probe and Comparison With the Flight Results. NASA paper presented at Second Symposium on the Plasma Sheath (Boston), Apr. 10-12, 1962.

8. Anon: Down-Range Anti-Ballistic Measurement Program (DAMP). Electromagnetic Wave Propagation and Radiation Characteristics of Anisotropic Plasmas. ARPA No. 51 (Contract DA 36-034-ORD-3144 RD), Radio Corp. of America, Apr. 1961.